Metallophysics and Advanced Technologies
Металофіз. новітні технол.
Metallofiz. Noveishie Tekhnol.
2023, vol. 45, No. 7, pp. 843–856
https://doi.org/10.15407/mfint.45.07.0843
Reprints available directly from the publisher

© 2023 G. V. Kurdyumov Institute for Metal Physics,
National Academy of Sciences of Ukraine
Published by license under
the G. V. Kurdyumov Institute for Metal Physics–
N.A.S. of Ukraine Publishers imprint.
Printed in Ukraine.

PACS numbers: 66.30.Lw, 68.35.Fx, 68.55.Ln, 72.15.-v, 81.15.Cd, 81.40.Cd, 82.80.Ms

Effect of Modulation Period on the Thermally-Induced Solid-State Reactions in Ni/Ti Thin Films

I. O. Kruhlov, N. V. Franchik, S. M. Voloshko, and A. K. Orlov

National Technical University of Ukraine
'Igor Sikorsky Kyiv Polytechnic Institute',
37 Peremohy Ave.,
UA-03056 Kyiv, Ukraine

In this work, we have studied the structure evolution of Ni/Ti layered stacks with a modulation period of 30 nm and 15 nm (total thickness of the stack is of 60 nm) deposited by RF magnetron sputtering onto *p*-Si (001) substrate upon vacuum annealing up to 700°C. As found based on the XRD, SIMS and four-point probe resistivity measurements' data, the diffusion-induced reactions in both stacks occur through the stages of metals' intermixing, amorphization and formation of intermetallic Ni_xTi phases. The application of a smaller modulation period leads to the more intense metals' intermixing, which results in the shift of the structural transitions onset to the lower temperatures. However, the modulation period does not influence the temperature range of amorphization, which is of ≅ 38°C for both stacks.

Key words: thin films, solid-state reactions, diffusion, crystal structure, amorphization.

В роботі досліджено зміну структури шаруватих плівкових композицій Ni/Ti з періодами модуляції у 30 нм і 15 нм (загальна товщина становить 60 нм), одержаних методом магнетронного осадження на підкладинки *p*-Si (001), в процесі відпалу у вакуумі до температури у 700°C. За результатами досліджень методами РСФА, МСВІ та чотирозондової резистометрії встановлено, що дифузійно-індуковані реакції в обох плівках перебігають через стадії перемішування металів, аморфізації та формування інтерметалідних фаз Ni_xTi. Зменшення періоду модуляції зумовлює інтенсифіка-

Corresponding author: Ivan O. Kruhlov, Andriy K. Orlov
E-mail: ivankruhlov@gmail.com, orlovandrii89@gmail.com

Citation: I. O. Kruhlov, N. V. Franchik, S. M. Voloshko, and A. K. Orlov, Effect of Modulation Period on the Thermally-Induced Solid-State Reactions in Ni/Ti Thin Films, *Metallofiz. Noveishie Tekhnol.*, **45**, No. 7: 843–856 (2023).
DOI: 10.15407/mfint.45.07.0843

цію дифузійних процесів між матеріялами шарів, що спричинює зменшення температур початку структурних перетворень. Водночас період модуляції не впливає на температурний інтервал аморфізації, який для обох плівок складає ≅ 38°C.

Ключові слова: тонкі плівки, твердотільні реакції, дифузія, кристалічна структура, аморфізація.

(Received 6 June, 2023; in final version, 24 June, 2023)

1. INTRODUCTION

NiTi alloy is the well-acknowledged material that has a pronounced shape memory effect due to the low-temperature martensite–austenite thermoelastic phase transition [1]. The reversible nature of this transition brings out a unique inelastic strain recovery effect which makes NiTi a promising material for engineering application in microelectromechanical (MEMS) devices such as microactuators, micropumps, *etc.* [2]. The application of NiTi thin films has become of especial relevance due to their fast response, competitively large transition forces, cooling rate and a strain recovery rate compared to the bulk material [3].

Basically, equiatomic NiTi thin films are obtained by magnetron co-sputtering from Ni and Ti high-purity targets on heated substrate [4] which allows easy control over deposition rate. However, phase transitions in NiTi alloys are very sensitive to composition, contamination, thermal treatment, and aging process, as well as sputtering conditions such as power, gas pressure, deposition temperature etc. [5]. Therefore, precise control over Ti and Ni atomic content ratio became a big challenge.

An alternative approach lies in the synthesis of the equiatomic NiTi alloy through a thermal treatment of the multilayered stack composed of alternately deposited Ni and Ti metal layers [6]. The increased number of individual metals nanolayers and variation of its modulation period leads to intensification of the formation of intermetallic compounds under elevated temperatures. This is due to the large negative Gibbs free energy of mixing in Ni/Ti multilayers which can be accompanied by exothermic reactions [7]. However, the modulation period cannot be reduced significantly because of the solid-state amorphization reaction at the Ni/Ti interface that leads to slowdown of further metals intermixing [8]. Cavaleiro *et al.* [9] studied the temperature ranges of $B2$ NiTi austenitic phase formation as a function of modulation period: the decrease of modulation period from 25 nm to 4 nm corresponded to the rise of reaction temperature from 320°C to 385°C. Clemens [10] revealed the change in Ni/Ti multilayered structure from polycrystalline to amorphous when moving the modulation period from 200 to 2 atomic planes. Cavaleiro *et al.* [7] analysed structural evolution with temperature of Ni/Ti multilayers with a modulation

period from 5 to 70 nm. The smaller modulation period has been applied, the more pronounced formation of disordered NiTi phase has been observed. Bhatt *et al.* [11] showed that the Ni/Ti interface amorphization is accompanied with the formation of Ni/Ni–Ti/Ti trilayer and the modified interface could be sufficiently thick and it expands with temperature up to 3.6 nm at 400°C. It has been shown that except for the modulation period, the order of Ti and Ni layers' deposition also strongly affects the diffusion-induced structural phase formation upon stacks' annealing [12].

However, most of the presented studies are devoted to the sufficiently thick multilayered structures (> 2 μm), which are related to their integration into MEMS devices. In present days, NEMS systems are actively developing, therefore the understanding of the effect of the modulation period on the diffusion-induced structural changes and phase composition in Ni/Ti stacks of nm-scale thicknesses is relevant. It became of especial importance for the films annealed to the elevated temperatures when the co-existence of numerous intermetallic Ni_xTi_y compounds may compromise the phase identification and understanding of composition distribution. In present work, the structural evolution of 60 nm thick Ni/Ti stacks with altered modulation period has been explored upon vacuum annealing.

2. METHODS AND OBJECTS

Two series of thin films were prepared, the bi-layered Ni (30 nm)/Ti (30 nm) and four-layered Ni (15 nm)/Ti (15 nm)/Ni (15 nm)/Ti (15 nm) stacks (hereinafter, $[Ni/Ti]_{x1}$ and $[Ni/Ti]_{x2}$, respectively) with an identical total thickness of 60 nm. Samples were fabricated using RF magnetron sputtering from high-purity Ni (99.99%) and Ti (99.99%) metal targets onto one-side polished *p*-type single-crystal Si (100) substrate at room temperature. Sputtering rate was adjusted to 10 nm/min for Ni at 300 W and Ti at 400 W, respectively. The thickness of the growing film was controlled using the quartz crystal microbalance. Before the deposition, silicon substrates were subjected to standard RCA cleaning procedure. No buffer layer such as SiO_2 or SiC was used prior to the film growth to explore if there is any effect of the metal layers' number on the film interaction with Si substrate at elevated temperatures.

After the deposition, thin films were annealed in a vacuum of 10^{-4} Pa in the temperature range from 200°C to 700°C for 30 minutes using a heating rate of 2°C/s. The temperature was measured using the *K*-type thermocouple mounted at the sample's surface.

For structure characterization and phase identification, x-ray diffraction (XRD) scanning was performed in θ–2θ Bragg–Brentano geometry using the Rigaku RINT (40 kV, 200 mA) diffractometer

equipped with 1.5405 Å CuK_α rotating anode. XRD patterns of the as-deposited and annealed films were recorded at room temperature with 0.05° step, applying the identical measurement parameters for all samples.

Chemical elemental depth profiling was performed using secondary ion mass spectrometry (SIMS) technique at MC-7201M device. Primary beam of Ar^+ ions of 10 keV energy was applied for the layer-by-layer elemental analysis. The discharge current of the gun was adjusted to 0.4 mA, current density was 2 μA/mm^2, and the background vacuum was $5.5 \cdot 10^{-5}$ Pa. In addition to the analysis of the in-depth secondary ions' distribution of the primary components (Ni^{28}, Ti^{22} and Si^{14}), the intensity of the secondary ions of C^{12} and O^{16} impurities was also registered.

For *in situ* monitoring of critical temperatures of solid-state transitions, the high-temperature four-point probe measurement technique has been applied [13]. The traditional sheet resistance measurement method was upgraded with a high-temperature four-point probe head. It provides the possibility to record the electrical resistivity as a function of temperature in the wide temperature range in a controlled environment. Thin film resistivity ρ is given by the equation [14]:

$$\rho = \frac{\pi}{\ln 2} t \frac{V}{I} = 4.5324 t \frac{V}{I}, \quad (1)$$

where t is the thickness of the film, V is the change in voltage measured between the inner probes, I is the current applied between the outer probes.

To simplify calculations and taking into account that the film is conductive, the direct current of 4.53 mA has been used. The probe spacing of 1.6 mm allows measuring samples less than 10×10 mm^2. The background pressure in the vacuum chamber is $5 \cdot 10^{-4}$ Pa. *In situ* resistivity test has been performed during heating up (with the rate of 1°C/s) the film up to approximately 550°C with automatically registration by the data logger. It is worth noting that the heating of the samples during resistometry test differs from the annealing conditions described earlier due to the difference of heating rate and absence of exposition at set temperature. The samples have been cooled down immediately after reaching 550°C in vacuum without exposition.

3. EXPERIMENTAL RESULTS

Figure 1, *a* shows the XRD patterns of the bi-layered $[Ni/Ti]_{\times 1}$ stacks after deposition and vacuum annealing in the temperature range from 200°C to 700°C given in the 2θ range from 35° to 55°. According to the XRD pattern, the phase composition of the bi-layered film after deposition consist of h.c.p. Ti and f.c.c. Ni phases represented by the Ti

(002) diffraction peak at 2θ angle of 37.74°, highly intense Ni (111) peak at 44.64° and weak Ni (200) peak at 52.08°. Such diffraction pattern, when Ni is formed with {111} fibre texture and Ti with {002} one, is typical for sputtered Ni/Ti multilayers [15, 16]. The substantial difference between the intensities of the Ni (111) and Ti (002) peaks is attributed to the higher crystallinity and texture of Ni layer compared to the Ti phase with a likely fine-grain structure. That is generally associated with the high chemical reactivity of Ti, which leads to the adsorption of background residual impurities (O, C, N, *etc.*) from vacuum chamber into the growing film during the magnetron sputtering.

As-deposited four-layered $[Ni/Ti]_{x2}$ stack shows almost similar XRD pattern (Fig. 1, *b*) to the one obtained from bi-layered stack. The difference lies in the broadening and slightly lower intensities of the diffraction peaks from both f.c.c. Ni and h.c.p. Ti phases for the stack with smaller modulation period. That is due to the fact that the smaller modulation period results in the finer mean crystallite size and higher defect density of the sputtered film.

The lattice spacings *d* for both $[Ni/Ti]_{x1}$ and $[Ni/Ti]_{x2}$ stacks calculated from the Ni (111) and Ti (002) peak positions using Gaussian fitting are summarized in Table 1. It is seen that the different modulation

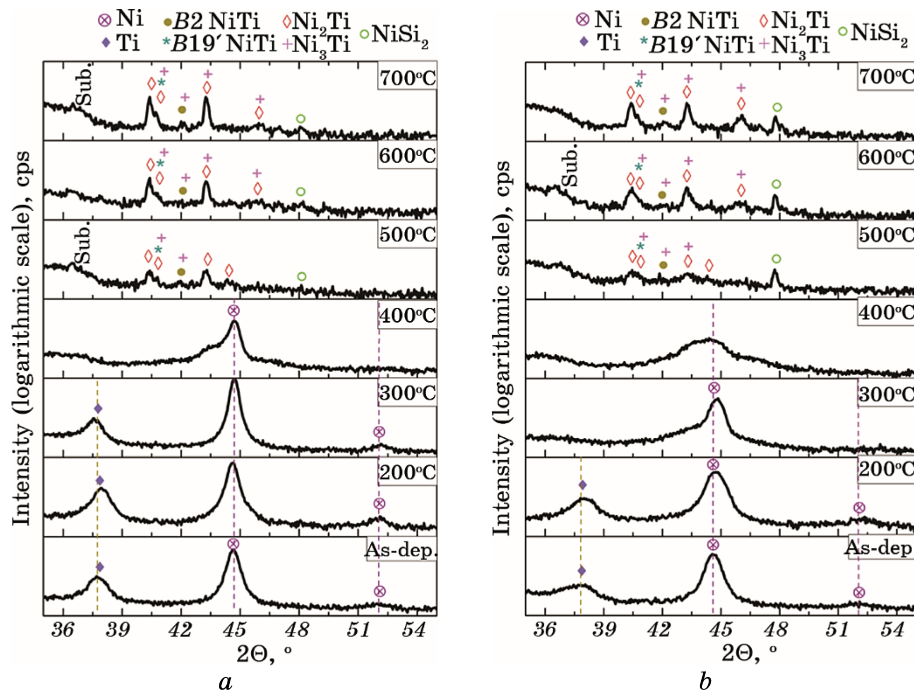

Fig. 1. XRD scans of the $[Ni/Ti]_{x1}$ (*a*) and $[Ni/Ti]_{x2}$ (*b*) stacks after deposition and after annealing in the temperature range 200–700°C.

TABLE 1. Lattice spacings d of f.c.c. Ni and h.c.p. Ti in Ni/Ti stacks with different modulation period after deposition and after annealing at 200°C and 300°C for 30 minutes.

Sample	$[Ni/Ti]_{\times 1}$		$[Ni/Ti]_{\times 2}$	
	d_{Ni111}, Å	d_{Ti002}, Å	d_{Ni111}, Å	d_{Ti002}, Å
As-deposited	2.028	2.383	2.030	2.400
Annealed at 200°C	2.030	2.370	2.025	2.369
Annealed at 300°C	2.026	2.397	2.022	—

period in as-deposited samples almost does not affect d_{Ni111} spacing (2.028 Å for 30 nm and 2.030 Å for 15 nm), while the d_{Ti002} spacing differs more significantly (2.383 Å for 30 nm and 2.400 Å for 15 nm). Comparing the calculated spacings to the bulk values, f.c.c. Ni lattice deviation is very slight (bulk $d_{Ni111} = 2.034$ Å [17]), whereas h.c.p. Ti lattice is significantly larger (bulk $d_{Ti002} = 2.342$ Å [17]). The distention of the Ti crystal structure in Ni/Ti multilayered films has been also reported in other works [15, 17]; it is generally associated with the high level of compressive mechanical stresses in the Ti sublayers oriented parallel to the metals' interface.

The chemical depth profiles of both films after deposition (Figure 2, *a*, *b*) confirms their multilayered structure consisting of Ni and Ti alternating layers (Ni as top layer). Despite the similar real thickness of each layer, the signal from Ti^{48} secondary ion at the depth profile is wider than for Ni^{58} one that is due to the higher sputtering yield of the latter. Besides the main elements (Ni^{58}, Ti^{48}, Si^{28}), the distribution of secondary ions of C^{12} and O^{16} impurities has also been registered. The moderate splash of intensity from impurities at the outer surface is related to their adsorption after taking the film out of the magnetron chamber to the atmosphere. The higher intensity of impurities at the surface for bi-layered stack compared to the four-layered one most likely indicates the higher level of contamination. It can be seen that after deposition the distribution of signal from both C^{12} and O^{16} impurities is more homogeneous through the depth of four-layered stack compared to the bi-layered one. It is also worth mentioning that due to the very limited diffusivities at room temperature, the splash of Si^{28} signal that can be seen at the surface cannot belong to the substrate. The origin of this splash is rather related to the surface carbohydrate

compounds with a similar atomic mass to the Si^{28} species.

Although the low-temperature annealing of both stacks at the 200°C almost does not lead to the considerable changes of their XRD patterns (Fig. 1), certain distinctions in the lattice spacings of metals due to the thermal evolution of stresses are observed (Table 1). It is also worth noting the appearance of slight asymmetry of the Ni (111) diffraction peak for the stack with smaller modulation period whose origin may be related to the onset of the interdiffusion processes.

Further increase of annealing temperature of four-layered stack to 300°C leads to the complete vanishing of Ti (200) diffraction peak and appearance of a new area of uneven intensity close to the position of Ni (111) fundamental reflection. Corresponding depth profile (Fig. 2, *d*) shows a distinct intermixing of Ni and Ti metals. The output of diffusion is the splash of Ti signal at the outer surface. It is known that Ni

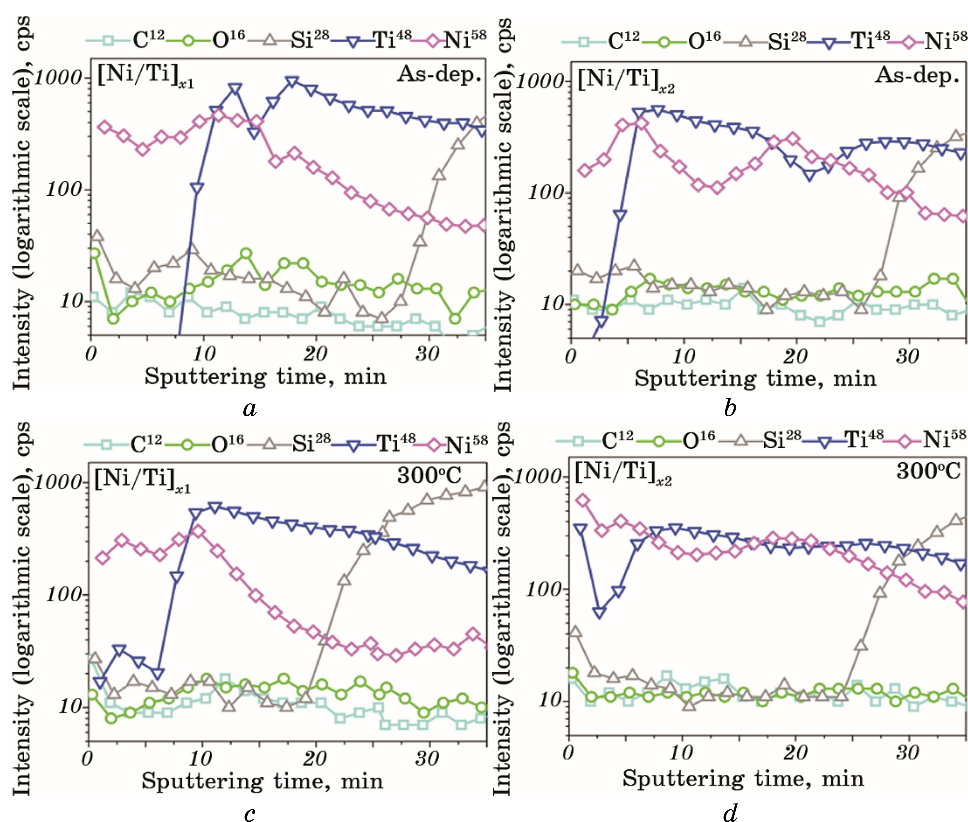

Fig. 2. SIMS depth profiles of the $[Ni/Ti]_{x1}$ and $[Ni/Ti]_{x2}$ stacks after deposition (*a*, *b*, correspondingly) and after annealing at 300°C (*c*, *d*) and 400°C (*e*, *f*). The signal from Ti^{48} secondary ions has been decreased 10 times for ease of analysis.

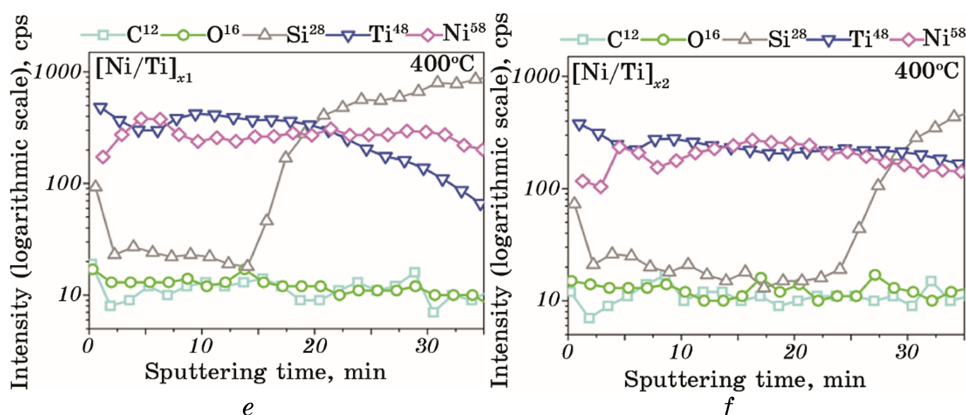

Continuation of Fig. 2.

diffusion occurs faster than Ti one in NiTi alloys [18] due to its much smaller activation enthalpy.

On the other hand, the profile of bi-layered stack (Fig. 2, *c*) demonstrates a much less intense layers' intermixing while its XRD scan shows no noticeable difference compared to the 200°C annealing. The development of diffusion between metals in a four-layered system leads to the first stages of a solid-state amorphization which gives a smoothed halo at 42–44° on the diffractogram well corresponding to the previously reported data for Ni/Ti stacks [11, 18]. It is worth recalling that the phenomenon of amorphization is typical for Ni/Ti layered stacks due to the high negative Gibbs energy of intermixing and anomalously fast diffusivity of f.c.c. Ni in h.c.p. Ti [19]. Typically, at the first stages this process develops through the layers' interface and along the grain boundaries. It is also seen at the depth profiles that the intense intermixing for a smaller modulation period results in the emergence of a pronounced Ti^{48} signal at the outer surface. Because of the more restrained intermixing in the stack with larger modulation period, the splash of Ti^{48} intensity in the near-surface area is also moderate. The accumulation of Ti at the surface is typically accompanied by the formation of TiO_x oxide due to the high affinity of Ti to O.

After next annealing at 400°C the amorphization is totally dominating in the four-layered stack. The corresponding XRD pattern (Fig. 1, *b*) shows no more diffraction peaks from crystalline f.c.c. Ni, only the blurred halo area from the amorphous phase is detected in the range of 42–47°. The depth profile exhibits the development of the diffusion processes that have been detected at lower temperatures earlier: (a) the further intermixing of Ni and Ti layers in the bulk of the stack leading to the almost homogeneous elemental distribution and (b) the formation of the Ni-free layer at the surface consisting of Ti phase only.

XRD pattern of the bi-layered stack after annealing at 400°C (Fig. 1, *a*) shows the similar diffraction pattern to the one obtained from the four-layered system annealed at 300°C. This indicates the first stage of diffusion-induced solid-state amorphization, which is confirmed by the intense metals' intermixing at the corresponding chemical profile (Fig. 2, *e*). Therefore, upon annealing of both films up to 400°C, the solid-state amorphization process is taking place in a similar manner, however this process starts earlier in the stack with a smaller modulation period. The smaller modulation period leads to the intensification of intermixing of the initial metal layers with earlier formation of the amorphous phase; however, it inhibits the development of the new intermetallic phases and their ordering.

One more fact that seems worth discussing is the shift of the signal from Si^{28} specie which is seen for the bi-layered film annealed at the temperatures of 300°C and 400°C. On the first glance, this may indicate the breaking of the integrity of the film/substrate interface. However, the following factors compromise this assumption: (a) the complete absence of any peaks from silicide phases at XRD scans at these temperatures and (b) the similar slope of Si^{28} signal at the interface with Ti for as-deposited and annealed films. Therefore, the film-substrate diffusion interaction is unlikely at these relatively low temperatures of thermal treatment. The observed shift may rather be the instrumental artefact related to the limited depth resolution of the method when dealing with tens nm-thick materials.

The significant changes in diffraction patterns of both stacks (Fig. 1) are detected after annealing at 500°C. A number of new diffraction peaks of moderate intensity in the range of 41–44° indicate that the amorphization stage observed at lower temperatures is followed by the stage of formation of new intermetallic NiTi compounds which is characteristic for both films. It follows from the analysis of the peaks' positions that the Ni_2Ti phase is dominating at these temperatures; however, its co-existence along with a small amount of Ni_3Ti intermetallic, austenitic *B*2 NiTi and martensitic *B*19′ NiTi phases cannot be excluded as well. Since there is no more trace of a blurred halo, it may be concluded that the complete bulk amorphization of the bi-layered stack is passing and completes within the temperature range from 400°C to 500°C. Notably, despite the earlier onset of intermixing and amorphization in a four-layered film, the similar intermetallic phases are formed in both stacks at 500°C. Moreover, it may be concluded from the analysis of the integral intensities of the diffraction reflections from intermetallic phases that their structure is less ordered in a film with a smaller modulation period. But the primary difference between the patterns of two stacks is the appearance of a clear peak at 47.75° for the case of four-layered film while for bi-layered stack this reflection is absent. The angular position of this reflection well corresponds

to the $NiSi_2$ silicide. This is well agreed with the fact that the formation of Ni silicides usually occurs at lower temperatures compared to the Ti ones [20].

Next increase of annealing temperature for both stacks up to 600°C is accompanied with the growth of intermetallic phases and their ordering which is indicated in the increased relative integral intensity of their diffraction peaks at the XRD scans (Fig. 1). It should be also noted the appearance of the $NiSi_2$ peak of low intensity for the four-layered stack. Therefore, the general behaviour of thermally-activated solid-state reactions in both stacks is similar, whereas the effect of modulation period is primarily evidenced in the shift of the temperatures of phase transitions onset. The smaller modulation period leads to the intensification of the diffusion intermixing of the initial metal layers in the stack which results in the lower temperatures of the onset of solid-state amorphization and silicide formation. For high annealing temperatures such as 700°C, there is no more difference in the phase composition of stacks with altered modulation period.

The obtained XRD and SIMS experimental data are well-agreed and have contributed to reveal the effect of the modulation period on the temperature shift of structural changes. However, the applied annealing temperature step of 100°C is not enough for precise determination of the temperature ranges of detected solid-state reactions. It is worth noting that determination of the exact phase transition temperatures of thin films is challenging due to their small volume-to-surface ratio. In this work, we additionally employed the high-temperature four-point probe measurement to monitor the phase transformations upon heating up to ≅ 520°C and cooling down in the vacuum conditions. The resulting *in situ* $\rho(T)$ curves shown in Fig. 3, *a*, *b* demonstrates the changes of films' electrical resistivity upon their heating and cooling.

The general behaviour of $\rho(T)$ resistivity curve for both films upon their heating is similar: its value gradually increases from $\cong 8\cdot 10^{-4}$ Ω·m at room temperature to $\cong 13\cdot 10^{-4}$ Ω·m at 280°C and then decreases to $\cong 3\cdot 10^{-4}$ Ω·m at 520°C. The origin of these dependencies is foremost attributed to the *p*-type semiconductor Si substrate for which an effect of majority carrier transition from extrinsic to intrinsic conduction (negative coefficient of resistance) is characteristic at elevated temperatures [21].

For ease of the analysis of structural transitions taking place in films as a function of annealing temperature, the high-temperature (350–500°C) part of the $\rho(T)$ curves for both stacks are plotted in Fig. 3, *c*. It consists of three regions with different slopes of the $\rho(T)$ curve which correspond to the three stages of solid-state reactions. It follows from the complex analysis of the XRD, SIMS and resistivity data that these stages may be summarized as following: (a) the I stage is associated with the metals intermixing which results in the process of inter-

facial amorphization, (b) the II stage corresponds to the bulk solid-state amorphization and (c) the III stage is attributed to the diffusion-induced formation of a new phases.

The effect of modulation period is evidenced in Fig. 3, *c* as the discrepancy of the temperatures of structural transitions. These results fit well to the already discussed XRD and SIMS data confirming the shift of the temperatures of solid-state reactions by decreasing the modulation period. The horizontal plateau which corresponds to the bulk amorphization starts at 400°C for $[Ni/Ti]_{x2}$ stack while for $[Ni/Ti]_{x1}$ film its onset is shifted to 426°C. It is also worth mentioning that the resistivity test revealed (Fig. 3, *c*) that the amorphization process occupies the same temperature range of 38°C for both stacks. The further increase of the temperature is accompanied with the gradual drop of resistivity which corresponds to the last stage of intermetallics formation and structure ordering. During cooling down, the $[Ni/Ti]_{x2}$

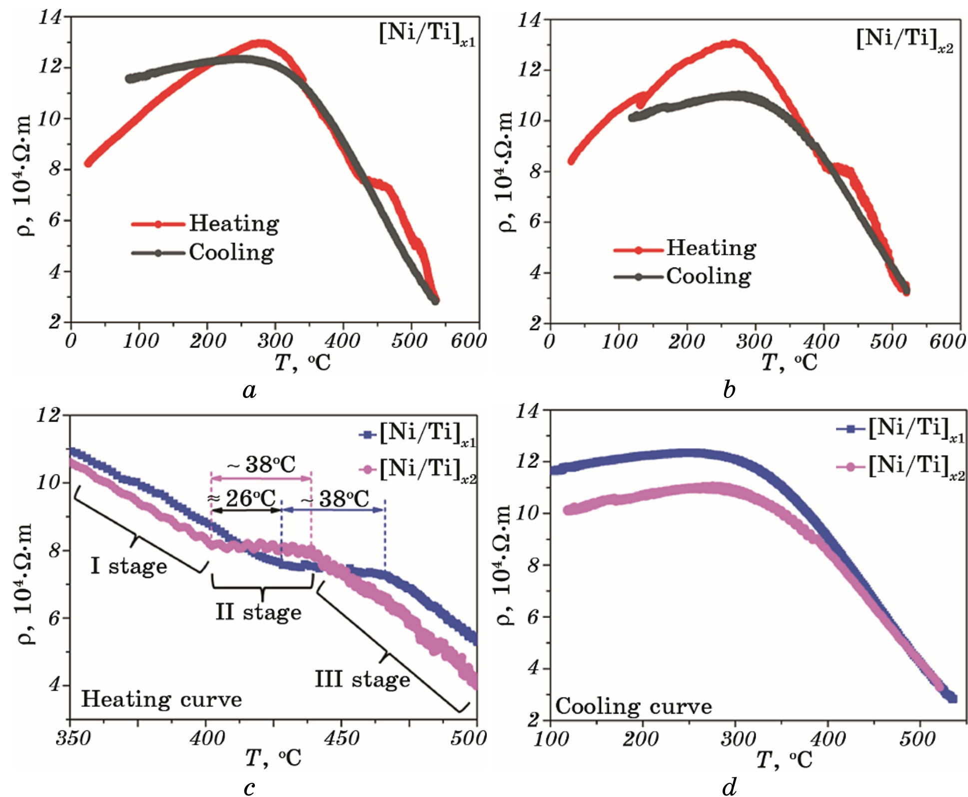

Fig. 3. Resistivity as a function of temperature $\rho(T)$ for $[Ni/Ti]_{x1}$ (*a*) and $[Ni/Ti]_{x2}$ (*b*) stacks. Figures *c* and *d* show plotted resistivity of both films upon heating and cooling, respectively.

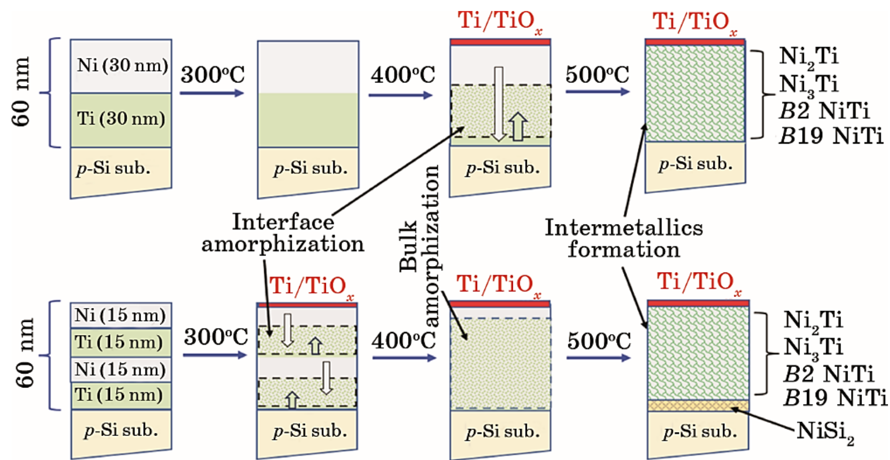

Fig. 4. Schematic illustration of the thermally-induced solid-state reactions in $[Ni/Ti]_{x1}$ and $[Ni/Ti]_{x2}$ stacks.

stack exhibits lower resistivity compared to the $[Ni/Ti]_{x1}$ one (Fig. 3, *d*). It can be due to the formation of Ni silicides at the film–substrate interface which according to the XRD data are already formed in $[Ni/Ti]_{x2}$ stack at 500°C (Fig. 1, *b*). It is acknowledged that the formation of a thin Ni silicide layer leads to decrease of contact resistance between film and Si substrate [22].

The sequence of thermally-induced solid-state reactions in Ni/Ti stacks studied by the combination of XRD, SIMS and four-point probe techniques is schematically summarized in Fig. 4. According to the SIMS and XRD data, diffusion intermixing and interface amorphization start at 100°C lower temperature in the system with smaller modulation period. The segregation of Ti atoms on the outer surface with likely formation of TiO_x oxide occurs earlier for smaller modulation periods as well. After annealing at 400°C, the bulk amorphization is characteristic for the structure of $[Ni/Ti]_{x2}$ stack, whereas, the interface amorphization occurs in $[Ni/Ti]_{x1}$ stack. The next rise of temperature to 500°C leads to the formation of Ni_xTi intermetallic phases in both stacks. For the $[Ni/Ti]_{x2}$ stack, this process is accompanied by the formation of $NiSi_2$ silicides due to the disruption of the film/substrate interface while for the $[Ni/Ti]_{x2}$ stack it starts only after annealing at higher temperatures.

4. CONCLUSIONS

Recent research in developing new materials for MEMS and NEMS applications shows a strong demand in synthesis of NiTi thin films with predefined properties. A promising way for the formation of NiTi thin

films with shape-memory effect is the thermally-induced intermixing of Ni and Ti in multilayered stacks composed of alternatively deposited metal layers. However, the relationship between modulation period and passing of the solid-state reactions remains unclear. Present study is devoted to figure out the effect of the modulation period of magnetron sputtered bi- and four-layered Ni/Ti films on the temperature intervals of solid-state reactions during annealing in vacuum in the temperature range from 200°C to 700°C. It follows from the results of XRD, SIMS and high-temperature four-point probe resistivity measurements that the solid-state reactions in both stacks are taking place in a few stages: (i) layers intermixing and interfacial amorphization, (ii) solid-state bulk amorphization, and (iii) formation of intermetallic phases. For a smaller modulation period, a more intense intermixing between metal layers results in the Ti segregation at the outer surface after annealing at 300°C. The application of in-situ four-point probe resistivity technique has revealed for the first time that despite the bulk amorphization starts at lower temperature for the stack with smaller modulation period (the shift is about 26°C), the duration of this process in both stacks is similar ($\cong$ 38°C).

This work was supported by the Grant (No. 0121U110283) from the Ministry of Education and Science of Ukraine. The authors would like to thank Dr. Tetsuya Ishikawa and Ms. Yasuko Matsumoto from the RIKEN SPring-8 Center, Japan for their invaluable support of present study.

REFERENCES

1. B. Reddy, *Results in Physics*, **17**: 103075 (2020).
2. J. M. Jani, M. Leary, A. Subic, and M. A. Gibson, *Mater. Design*, **56**: 1078 (2014).
3. J. J. Gill, D. T. Chang, L. A. Momoda, and G. P. Carman, *Sensors and Actuators A: Physical*, **93**, No. 2: 148 (2001).
4. A. Kumar, D. Singh, and D. Kaur, *Surf. Coat. Technol.*, **203**, No. 12: 1596 (2009).
5. H. Cho, H. Y. Kim, and S. Miyazaki, *Sci. Technol. Adv. Mater.*, **6**, No. 6: 678 (2005).
6. T. Lehnert, S. Tixier, P. Böni, and R. Gotthardt, *Mater. Sci. Eng. A*, **273**: 713 (1999).
7. A. J. Cavaleiro, R. J. Santos, A. S. Ramos, and M. T. Vieira, *Intermetallics*, **51**: 11 (2014).
8. R. Gupta, M. Gupta, S. K. Kulkarni, S. Kharrazi, A. Gupta, and S. M. Chaudhari, *Thin Solid Films*, **515**, No. 4: 2213 (2006).
9. A. J. Cavaleiro, A. S. Ramos, R. M. S. Martins, F. B. Fernandes, J. Morgiel, C. Baehtz, and M. T. Vieira, *J. Alloys Comp.*, **646**: 1165 (2015).
10. B. M. Clemens, *Phys. Rev. B*, **33**, No. 11: 7615 (1986).
11. P. Bhatt, A. Sharma, and S. M. Chaudhari, *J. Appl. Phys.*, **97**: 043509 (2005).

12. A. K. Orlov, I. O. Kruhlov, I. E. Kotenko, and S. M. Voloshko, *Metallofiz. Noveishie Tekhnol.*, **45**, No. 1: 55 (2023).
13. T. Duguet, F. Senocq, L. Aloui, F. Haidara, D. Samélor, D. Mangelinck, and C. Vahlas, *Surf. Interface Analysis*, **44**, No. 8: 1162 (2012).
14. F. Smits, *Bell System Technical J.*, **37**, No. 3: 711 (1958).
15. H. Aboulfadl, F. Seifried, M. Stueber, and F. Muecklich, *Mater. Lett.*, **236**: 92 (2019).
16. S. Petrović, D. Peruško, M. Mitrić, J. Kovac, G. Dražić, B. Gaković, K. P. Homewood, and M. Milosavljević, *Intermetallics*, **25**: 27 (2012).
17. W. L. Johnson, *Prog. Mater. Sci.*, **30**, No. 2: 81 (1986).
18. S. V. Divinski, I. Stloukal, L. Kral, and C. Herzig, *Defect and Diffusion Forum*, **289–292**: 377 (2009).
19. L. Scotti, N. Warnken, and A. Mottura, *Acta Mater.*, **177**: 68 (2019).
20. M. K. Rahman, F. Nemouchi, T. Chevolleau, P. Gergaud, and K. Yckache, *Mater. Sci. Semiconductor Processing*, **71**: 470 (2017).
21. S. Lundgaard, S. H. Ng, D. Cahill, J. Dahlber, D. Ruan, N. Cole, P. Stoddart, and S. Juodkazis, *Technologies*, **7**, No. 4: 75 (2019).
22. E. Bourjot, M. Putero, C. Perrin-Pellegrino, P. Gergaud, M. Gregoire, F. Nemouchi, and D. Mangelinck, *Microelectronic Eng.*, **120**: 163 (2014).